

Earthquake processes of the Himalayan collision zone in eastern Nepal and the southern Tibetan Plateau

T. L. de la Torre,¹ G. Monsalve,¹ A. F. Sheehan,¹ S. Sapkota² and F. Wu³

¹University of Colorado at Boulder, Cooperative Institute for Research in the Environmental Sciences, Campus Box 399, 2200 Colorado Blvd., Boulder, CO 80309, USA. E-mail: Thomas.Delatorre@colorado.edu

²Department of Mines and Geology, Nepal

³State University of New York at Binghamton

Accepted 2007 June 26. Received 2007 June 26; in original form 2007 January 19

SUMMARY

Focal mechanisms determined from moment tensor inversion and first motion polarities of the Himalayan Nepal Tibet Seismic Experiment (HIMNT) coupled with previously published solutions show the Himalayan continental collision zone near eastern Nepal is deforming by a variety of styles of deformation. These styles include strike-slip, thrust and normal faulting in the upper and lower crust, but mostly strike-slip faulting near or below the crust–mantle boundary (Moho). One normal faulting earthquake from this experiment accommodates east–west extension beneath the Main Himalayan Thrust of the Lesser Himalaya while three upper crustal normal events on the southern Tibetan Plateau are consistent with east–west extension of the Tibetan crust. Strike-slip earthquakes near the Himalayan Moho at depths >60 km also absorb this continental collision. Shallow plunging *P*-axes and shallow plunging EW trending *T*-axes, proxies for the predominant strain orientations, show active shearing at focal depths ~60–90 km beneath the High Himalaya and southern Tibetan Plateau. Beneath the southern Tibetan Plateau the plunge of the *P*-axes shift from vertical in the upper crust to mostly horizontal near the crust–mantle boundary, indicating that body forces may play larger role at shallower depths than at deeper depths where plate boundary forces may dominate.

Key words: focal mechanisms, Tibetan Plateau, earthquake depths, The Himalaya, Nepal, continental collision.

1 INTRODUCTION

Do earthquakes occur in the upper mantle or only in the crust of continental lithosphere? In the Himalayan convergence zone, a bimodal distribution of brittle strength in the crust and upper mantle with a ductile transition in the lower crust has been used to explain the existence of subcrustal hypocentres under the southern Tibetan Plateau (e.g. Chen & Molnar 1983; Chen & Kao 1996; Zhu & Helmberger 1996; Chen & Yang 2004). Other authors have suggested that elastic thicknesses of continents are less than or equal to the seismogenic thickness, that both are less than the crustal thickness, and that continental earthquakes occur in the crust while the upper mantle deforms as a weaker ductile layer (e.g. Maggi *et al.* 2000a; Jackson 2002a,b; Jackson *et al.* 2004; McKenzie *et al.* 2005; Mitra *et al.* 2005). Both sides of this controversy use the hypocentres and focal mechanisms of many of the same earthquakes in their interpretations of the continental lithosphere in the Himalayan region. Determining the source parameters of additional earthquakes and careful analysis of their focal depths near the crust–mantle boundary provide further fuel for this controversy.

Studies using *P*-wave first motions, synthesis of body waves and moment tensor inversions of earthquakes show largely underthrusting, east–west and north–south extension in the shallow crust

beneath the Himalaya and the southern Tibetan Plateau (Chen & Molnar 1983; Baranowski *et al.* 1984; Molnar & Lyon-Caen 1989; Randall *et al.* 1995; Kumar 1998) as well as strike-slip and east–west extension at depths >70 km under the southern Tibetan Plateau (Chen *et al.* 1981; Molnar & Chen 1983; Zhu & Helmberger 1996; Harvard University Department of Geological Sciences 2005). These solutions represent much of the focal mechanism record in the Himalaya and the southern Tibetan Plateau (Tables 1 and 2). Analysis of earthquakes recorded by a local seismic network can provide Himalayan deformation information which might be missed by analysis of intermittent earthquakes detectable teleseismically.

The Himalayan Nepal Tibet Seismic experiment (HIMNT) was a seismic network of 29 broad-band stations deployed in 2001–2003 (Fig. 1). In this paper, we analyse earthquake source parameters for 17 of the best quality events recorded by the HIMNT network (Fig. 2). We supplement the HIMNT data with data from the broad-band experiment in western Bhutan in 2002–2003 (Velasco *et al.* 2007), data from the Global Seismic Network station LSA in Lhasa, China, and short period vertical component data from the permanent seismic network of the Department of Mines and Geology Nepal. We determine fault parameters, which are cross checked with first motion polarities, and focal depths using a moment tensor inversion

Table 1. Fault Plane Solutions from previous studies.

No.	Date	Lat °N	Lon °E	Depth km	Mag.	P az.	P pl.	T az	T pl.	Source
1	1/12/1965	27.4	87.84	15	5.9 M_b^a	180	30	0	60	No. 3 Baranowski <i>et al.</i> (1984)
2	8/1/1973	29.59	89.17	85	4.9 M_b^a	184	37	89	6	No. 8 Molnar and Chen (1983)
3	3/24/1974	27.73	86.11	16	4.8 M_b^a	185	43	5	47	No. 9 Baranowski <i>et al.</i> (1984)
4	9/14/1976	29.78	89.54	90	5.4 M_b^a	185	72	290	5	Chen <i>et al.</i> (1981)
5	6/19/1979	26.74	87.48	21	5.2 M_b^a	103	86	341	2	No. 23 Ni & Barazangi (1984)
6	11/19/1980	27.39	88.80	44	6.0 M_b^a	166	15	73	12	No. 59 Ekström (1987) ¹
7	1/10/1986	28.66	86.57	85	5.5 M_b^a	348	40	96	20	No. 134 Ekström (1987) ¹
8	8/20/1988	26.73	86.59	51	6.4 M_b^a	209	35	65	49	No.T9 Chen and Yang (2004)
9	12/21/1991	27.90	88.14	70	4.7 M_w	157	6	252	3	No.355 Zhu & Helmberger (1996)
10	3/7/1992	29.44	89.37	80	4.2 M_w	210	27	303	3	No.67 Zhu & Helmberger (1996)
11	4/4/1992	28.15	87.98	80	4.8 M_w	6	31	277	3	No.95 Zhu & Helmberger (1996)
27	1/31/1997	28.06	85.34	13	5.9 M_L^b	312	30	181	58	Kumar (1998)

Note: Summary of the focal mechanisms from 1965 to 2005 within our study region. We replaced the hypocentres of the moment tensor solutions from the Harvard Centroid Moment Tensor catalog with the hypocentres labelled DEQ from the EHB catalog (Engdahl *et al.* 1998).

^aFrom Chen & Yang (2004).

^bFrom Pandey *et al.* (1999).

Table 2. Harvard CMT events with hypocentres from the EHB catalogue (Engdahl *et al.* 1998).

No.	Date	Lat °N	Lon °E	Depth km	Mag.	P az.	P pl.	T az	T pl.
12	10/29/1988	27.87	85.65	13.7	5.2 M_w	205	16	353	71
13	4/9/1989	29.16	90.06	11.2	5.1 M_w	155	70	260	5
14	3/20/1993	29.01	87.36	14.1	6.2 M_w	355	68	92	3
15	3/20/1993	29.02	87.36	16.1	5.1 M_w	273	60	83	30
16	7/3/1996	30.08	88.14	5.3	5.6 M_w	356	82	90	1
17	7/3/1996	30.12	88.21	45.2	5.0 M_w	249	72	80	18
18	7/31/1996	30.20	88.16	12.1	5.4 M_w	25	58	258	21
19	11/3/1997	29.05	85.41	9.5	5.5 M_w	61	72	276	15
20	7/20/1998	30.17	88.22	11.6	5.7 M_w	85	76	281	13
21	7/21/1998	30.27	88.18	10.3	5.0 M_w	124	88	304	2
22	8/25/1998	30.25	88.17	20.4	5.8 M_w	2	74	268	1
23	8/28/1998	30.26	88.26	25.0	5.0 M_w	0	90	289	0
24	9/30/1998	30.05	88.11	12.0	5.1 M_w	285	71	65	15
25	10/5/1998	30.24	88.26	38.8	5.2 M_w	85	72	286	17
26	3/26/2005	28.44	87.846	78.0	4.7 M_w	331	19	68	20

Note: Summary of the focal mechanisms from 1965 to 2005 within our study region. We replaced the hypocentres of the moment tensor solutions from the Harvard Centroid Moment Tensor catalogue with the hypocentres labelled DEQ from the EHB catalogue (Engdahl *et al.* 1998).

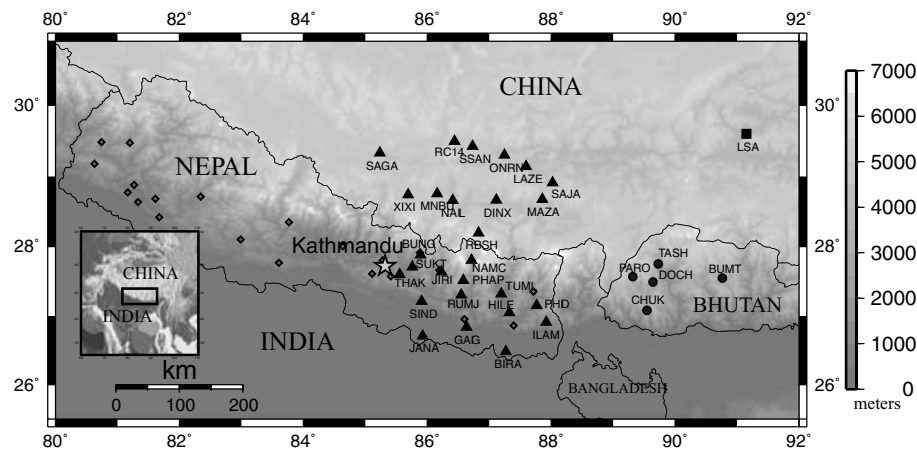


Figure 1. Station locations of the Himalayan Nepal Tibet Seismic Experiment (HIMINT), a Program for Array Seismic Studies of the Continental Lithosphere (PASSCAL) broadband seismic project of the University of Colorado at Boulder, Binghamton University, the Department of Mines and Geology of Nepal, and the Institute of Geology and Geophysics of the Chinese Academy of Science. Triangles are HIMINT broadband station locations, circles are broadband stations from the 2002 to 2003 Bhutan experiment (Velasco *et al.* 2007), diamonds are stations of the National Seismological Network of Nepal, and the square is GSN station LSA. Grey scale signifies topography in meters.

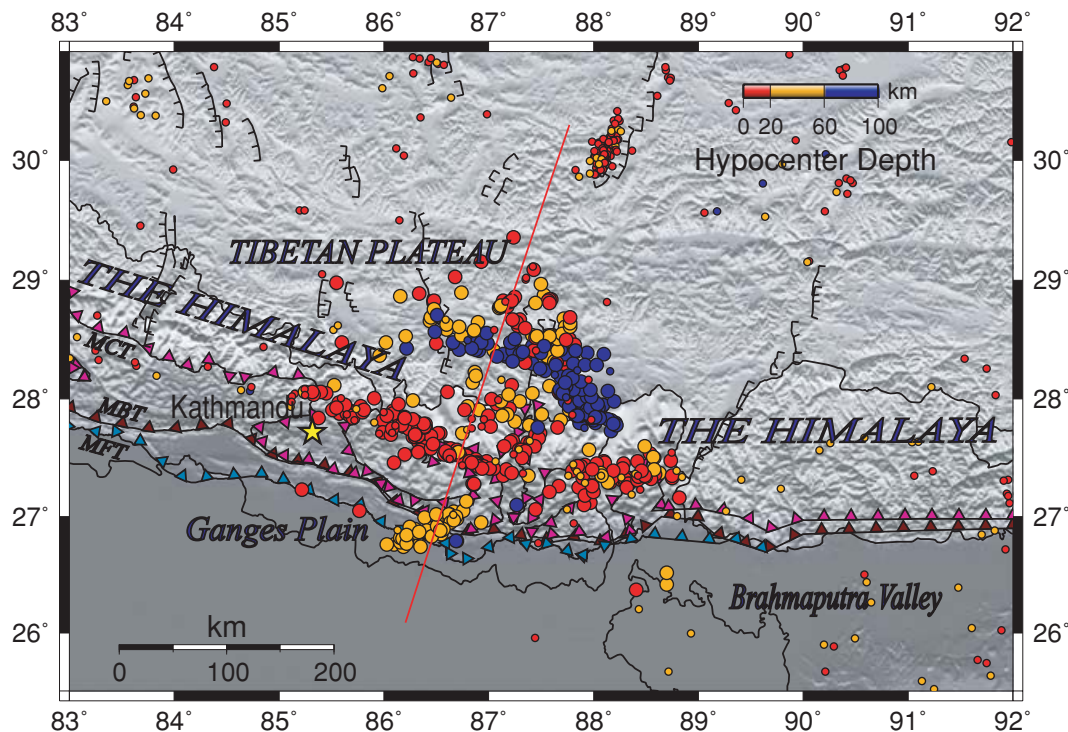


Figure 2. Subset of seismicity from 2001 October to 2003 April located by HIMNT (Monsalve *et al.* 2006) (large circles) and earthquakes from 1964 to 2005 of the EHB catalogue (Engdahl *et al.* 1998) (small circles). Note three distinct groups of seismicity: (1) along the Himalayan Front <20 km focal depth, (2) in southern Nepal at 20–60 km depth and (3), beneath the Himalaya and the Tibetan Plateau at >60 km depth. Barbed lines along the Himalayan Front represent approximate locations of the Main Central Thrust (MCT), the Main Boundary Thrust (MBT), and the Main Frontal Thrust (MFT). Normal faults on the Tibetan Plateau are spiked lines. Red line denotes cross section in Fig. 4.

method. These results are combined with previously published focal mechanisms to describe the seismotectonics of the Himalayan region (Figs 3 and 4). Nine of the earthquakes presented here were at focal depths near the crust–mantle boundary and the hypocentres and deformation styles of these earthquakes are examined in detail.

2 MICROEARTHQUAKE PATTERN UNDER THE EASTERN NEPAL HIMALAYA AND SOUTHERN TIBETAN PLATEAU

Earthquakes recorded during the 2001–2003 HIMNT deployment range in magnitude from M_L 2.0–5.0 and have hypocentres in three distinct spatial groups (Fig. 2) (Monsalve *et al.* 2006). The first group is a narrow band of earthquakes at hypocentral depths <20 km following the curved Himalayan front. The same pattern was observed with the microearthquakes recorded by the permanent network of the Department of Mines and Geology of Nepal (Pandey *et al.* 1999). Pandey *et al.* (1999) suggest that this seismicity reflects deformation between the upper and lower crust at a ramp under the Lesser and High Himalaya. This ramp is suggested to be locked near a depth of 20 km, where stress accumulates until it is released by a large earthquake similar to the Bihar 1934 earthquake (Bilham *et al.* 1997; Cattin & Avouac 2000; Feldl 2005).

The second group of earthquakes is a narrow NE–SW trending cluster at 30–70 km hypocentral depth beneath southeastern Nepal. This is similar to a cluster noted by Pandey *et al.* (1999). Pandey *et al.* (1999) concluded that this group includes aftershocks of the 1988 August 20 m_b 6.4 Udayapur earthquake (No. 8, Table 1). The

Udayapur earthquake occurred at a depth of 51 ± 5 km (Chen & Kao 1996). Our cluster of events in this region shows no M_L decrease, nor a decline in the amount of earthquakes through time. These earthquakes may represent deformation of the same active structure that generated the Udayapur event, rather than Udayapur aftershocks.

Another pattern in the local seismicity is a cluster at depths >60 km trending WNW to ESE beneath the High Himalaya and southern Tibetan Plateau. The hypocentres are close to the crust–mantle boundary and depths of selected events are further analysed here and in Monsalve *et al.* (2006).

3 STRUCTURES UNDER THE HIMALAYA AND THE TIBETAN PLATEAU

The main structural feature in the Himalayan region in eastern Nepal and southern China can approximately be thought of as a wedge that contains the Himalayan Mountains underthrust by the India Shield on a decollement, called the Main Himalayan Thrust (e.g. Zhao & Nelson 1993; Bollinger *et al.* 2004). The active portion of the Main Himalayan Thrust pierces the surface at the Main Frontal Thrust just south of the sub-Himalayan fold belt and absorbs ~ 21 mm yr^{-1} of shortening beneath the India crust and the Himalaya (Lave & Avouac 2000). The southern Tibetan Plateau near the Himalaya geologically shows normal faulting with E–W extension in the vicinity of the Indus–Tsangpo Suture Zone (Armijo *et al.* 1986; Fig. 3). Focal mechanisms along the Himalayan front (Table 1) indicate that intermediate to large magnitude thrust earthquakes accommodate

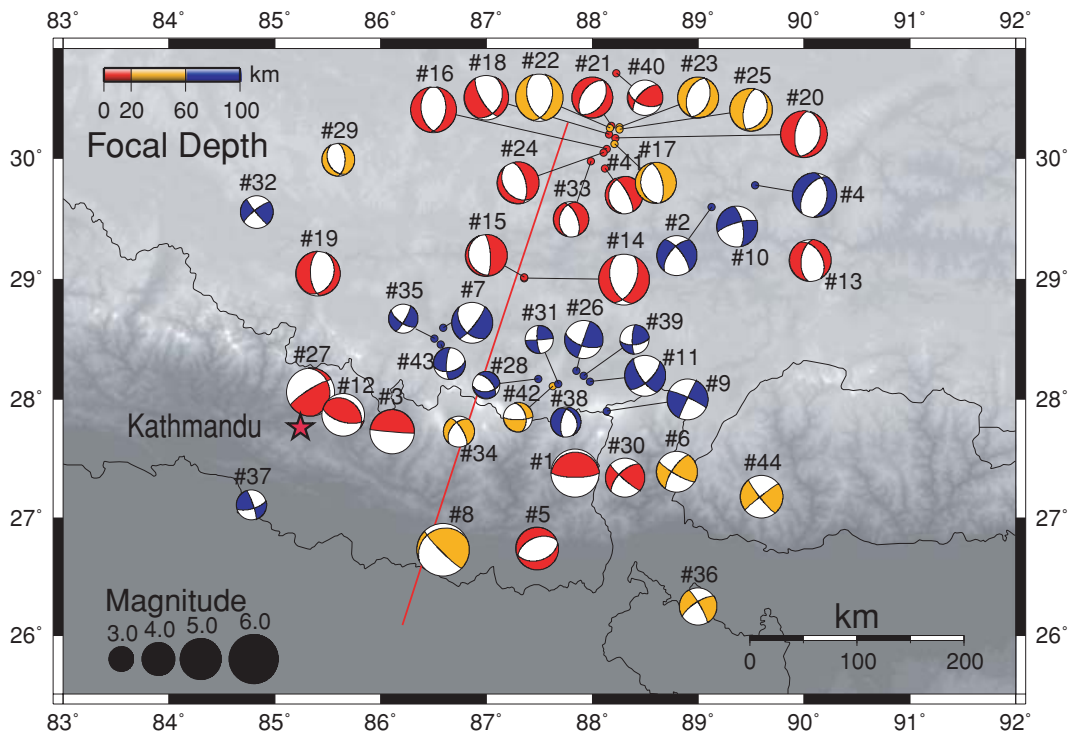


Figure 3. Focal mechanisms from this study and previous studies. Nos. 1–11 and 27 are plotted at their published depths, Nos. 12–26 from the Harvard CMT catalog are plotted at the hypocentral locations from the EHB Catalogue (Engdahl *et al.* 1998), Nos. 28–44 are plotted at their minimum misfit focal depth (Table 3). Depth (colour) and magnitude (size) of the focal mechanisms are indicated. Red line denotes cross section in Fig. 4.

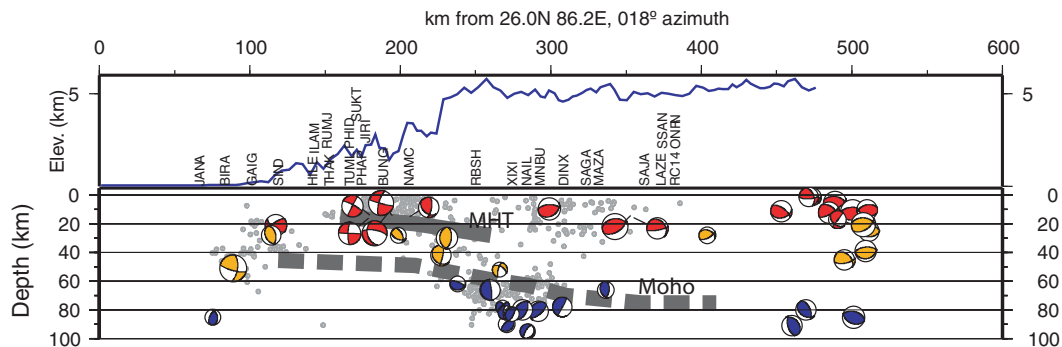


Figure 4. 600 km cross section from 26.0N 86.2E azimuth 018° showing the 2001–2003 seismicity detected by HIMNT and the focal mechanisms in back projection. Grey lines denote the Main Himalayan Thrust (MHT) and the Moho from Schulte-Pelkum *et al.* (2005). Approximate bounds for the Moho of ± 5 km denoted by line thickness. Focal mechanisms coloured by depth and magnitude as in Fig. 3. Regional topography is plotted above the seismicity with approximate locations of HIMNT stations. Note the strike-slip motion at or below the Moho, particularly in the cluster beneath the Himalaya.

shortening along the Himalaya at depths <30 km (Ni & Barazangi 1984; Molnar & Lyon-Caen 1989; Kayal 2001). Moho depths under the Himalaya and the Tibetan Plateau have been inferred from receiver function studies. Yuan *et al.* (1997) report Moho depths from ~70 km at ~28°N, 090°E slightly north of the Himalaya to 80 km at ~30°N under seismic station LSA (Lhasa, China). Mitra *et al.* (2005) infer 40–50 km Moho under the Himalaya in northeast India ~400 km east of the HIMNT network, a 60–70 km Moho near ~28°N, 090°E, and an 88 km Moho under station LSA. Schulte-Pelkum *et al.* (2005) imaged the Moho at 45–48 km under the sub-Himalaya in eastern Nepal, steepening to a 15° dip north under the High Himalaya and then flattening at 75 km before 29.5°N, 087.5°E.

We plot the focal depths from our moment tensor inversions with respect to the crust–mantle boundary imaged by Schulte-Pelkum

et al. (2005) (Fig. 4). We use the Moho of Schulte-Pelkum *et al.* (2005) for two reasons: (1) their cross section transects the same area where the earthquakes analysed here are located and (2) we use the same crust and upper-mantle seismic velocity models as they did so that depth comparisons with our moment tensor solutions are internally consistent.

4 MOMENT TENSOR INVERSION AND FIRST MOTION POLARITIES

Moment tensor inversion of seismic waveforms allows one to calculate the fault plane solution as well as estimate focal depth and seismic moment of earthquakes. Most of the earthquakes within the HIMNT network were too small for moment tensor inversion

Table 3. Fault plane solutions of earthquakes detected by HIMNT from 2001 to 2003.

No.	Date	Lat °N	Lon °E	M ^w	Depths ¹ km			Solution with minimum misfit						Average solutions within minimum misfit + 0.10							
					Model	Depth ² km	P-axis°		T-Axis°		Depth (km) ²		P Az.°		P Pl.°		T Az.°		T Pl.°		
							Az.	Pl.	Az.	Pl.	Mean	±	Mean	±	Mean	±	Mean	±	Mean	±	
28	10/19/01	28.17	87.49	3.3	68 ± 3	M1	78	284.9	57.4	23.1	5.2	80	9	277	15	61	9	42	54	7	4
29	11/7/01	29.99	85.60	4.0	1 ± 2	M2	22	313.4	73.8	79.1	9.6	23	10	279	57	80	7	78	5	5	4
30	12/2/01	27.34	88.31	4.8	22 ± 1	M2	13	181.3	13.4	84.8	25.5	16	8	182	2	16	2	85	2	22	8
31	1/5/02	28.13	87.68	3.4	76 ± 2	M2	82	131.9	8.6	40.2	11.1	76	11	165	70	11	5	106	87	8	5
32	3/7/02	29.56	84.83	4.0	80 ± 1	M1	66	186.8	4.5	95.8	12.2	69	15	142	110	7	4	113	51	13	9
33	3/23/02	29.98	87.99	4.3	1 ± 3	M2	1	209.2	67.6	81.8	14.0	5	4	190	13	45	18	73	11	27	17
34	5/2/02	27.73	86.74	3.8	26 ± 1	M2	28	195.4	46.2	88.7	15.4	31	12	195	3	43	3	89	1	16	2
35	5/8/02	28.51	86.51	3.6	84 ± 1	M1	83	344.6	25.9	79.2	9.3	84	8	290	79	15	8	82	2	14	4
36	6/20/02	26.25	89.00	4.6	25 ± 3	M2	28	194.9	19.3	102.5	6.7	33	14	195	1	20	1	103	1	6	2
37	7/2/02	27.11	84.78	3.7	59 ± 3	M2	84	29.1	8.8	295.8	20.6	84	5	30	3	12	4	296	4	18	3
38	7/16/02	27.81	87.75	3.7	67 ± 2	M1	62	134.5	65.5	267.6	17.3	62	8	138	6	64	2	268	3	17	3
39	7/18/02	28.20	87.92	3.6	85 ± 3	M1	93	309.8	10.2	46.0	30.9	90	4	310	1	10	1	45	1	29	2
40	8/22/02	30.07	88.23	4.3	1 ± 3	M2	17	345.3	5.5	81.9	49.7	20	11	251	79	10	18	79	4	50	9
41	8/31/02	29.92	88.12	4.7	1 ± 1	M1	1	226.6	59.3	70.8	28.5	6	5	208	13	47	9	71	1	33	4
42	10/29/02	28.11	87.63	3.6	67 ± 1	M1	52	316.7	40.4	211.2	17.3	60	11	314	2	31	8	211	4	22	8
43	2/26/03	28.46	86.57	3.9	81 ± 3	M2	73	50.1	40.8	305.4	16.4	77	9	47	8	32	8	254	83	10	7
44	3/25/03	27.18	89.60	5.2	-	M2	28	6.4	2.7	96.8	7.5	33	8	6	1	2	1	97	1	6	2

Note: Focal depths of minimum misfit solutions are either from the M1 or M2 seismic velocity models. Mean solutions are average of solutions from both M1 and M2 models that are within 0.10 of the minimum misfit solution. Broad minimum misfit versus depths curves account for large standard deviations of the focal depths (≥ 10 km) and P/T axes.

^aTraveltime inversion depths, relative to sea level.

^bCorrected relative to sea level.

of data from stations at teleseismic distances. We invert waveforms from local and regional stations which allows us to determine fault plane solutions even for events recorded at only a few stations and with gaps in azimuthal coverage (Randall *et al.* 1995; Ichinose *et al.* 2003; Stich *et al.* 2003, 2005).

We calculate moment tensor inversions for 17 earthquakes using the method of Ammon & Randall (1994) (Figs 3 and 4) (Table 3). The method follows from Jost and Herrmann (1989) where a 1-D velocity model and a point source at a fixed hypocentre are assumed. The inversion is combined with a grid search over depth to obtain the focal mechanism solution and focal depth with the minimum least squares misfit error between observed and synthetic seismograms. Green's functions are created using the reflectivity method of Randall (1994). We solve for five moment tensor elements, M_{xx} , M_{yy} , M_{xy} , M_{xz} and M_{yz} , assuming a purely deviatoric moment tensor. The sixth element, M_{zz} , is constrained to $(1) M_{zz} = -(M_{xx} + M_{yy})$ (Jost & Herrmann 1989). With this constraint, compensated linear vector dipole (CLVD) components, a special class of non-double-couple sources, are allowed.

4.1 Earth models

Since crustal thickness and topography vary dramatically across the study region, we use four different velocity models for the inver-

sions, two for the Nepal/Himalayan region and two for the southern Tibetan Plateau. Our M1 model uses the Nepal/Himalayan velocity model and the Tibetan Plateau velocity model from Monsalve *et al.* (2006) (Table 4). Our M2 model uses the Nepal/Himalayan velocity model and the Tibetan Plateau model of Schulte-Pelkum *et al.* (2005) (Table 4). We assume the epicentres determined from Monsalve *et al.* (2006) in the moment tensor analysis. We present results generated using the M1 and M2 models because they were the structures used for the epicentre relocations (Monsalve *et al.* 2006) and in the receiver function analysis that produced our reference Moho depths (Schulte-Pelkum *et al.* 2005). For the earthquakes located under the Ganges Plain, the Lesser Himalaya and the High Himalaya, we use the Nepal/Himalayan velocity models to model seismograms from stations south of 28°N, and the Tibetan Plateau velocity models for seismograms from stations north of 28°N. For earthquakes north of 29°N, the Tibetan Plateau velocity models are used exclusively.

4.2 The moment tensor method

We chose earthquakes based on preliminary magnitudes and visually good signal to noise on the seismograms. We concentrate much of this analysis on the deep seismic cluster under the High Himalaya and the southern Tibetan Plateau and the shallow frontal earthquakes

Table 4. Earth models.

	Thickness (km)	V_p (km s ⁻¹)	V_s (km s ⁻¹)
Model M1	3	5.5	3.2
Eastern Nepal	20	5.7	3.2
(Monsalve <i>et al.</i> 2006)	32	6.3	3.7
	–	8	4.5
Southern Tibetan Plateau	3	5.8	3.3
(Monsalve <i>et al.</i> 2006)	37	5.8	3.5
	30	6.9	4
	–	8.6	4.9
Model M2 Eastern Nepal	20	5.7	3.3
(Schulte-Pelkum <i>et al.</i> 2005)	28	6.3	3.7
	–	8.1	4.7
Southern Tibetan Plateau	40	5.5	3.4
(Schulte-Pelkum <i>et al.</i> 2005)	35	7.4	4.3
	–	8.1	4.7

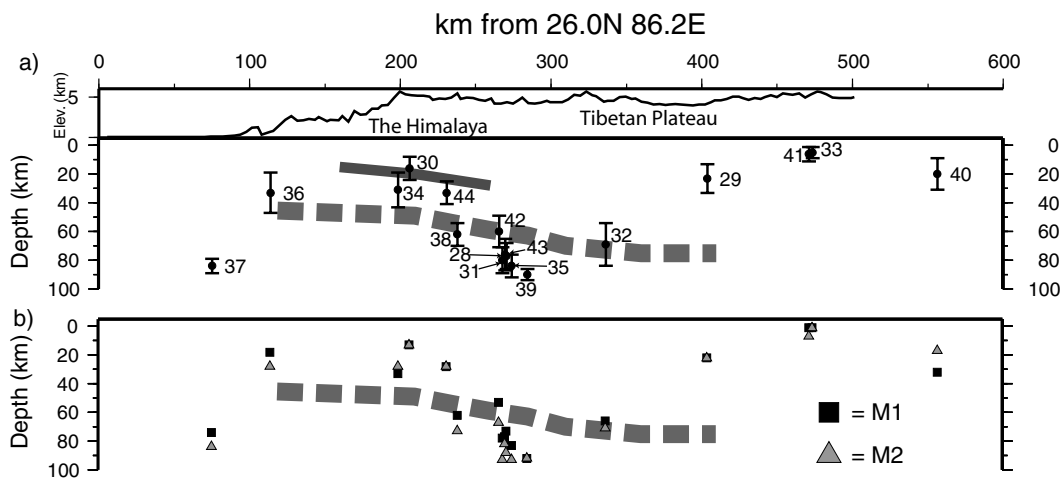


Figure 5. (a) Average focal depths with standard deviation bounds (Table 3) plotted in same cross section as Fig. 4. Solid and dashed lines denote the Main Himalayan Thrust and the Moho, ± 5 km (line thickness), from Schulte-Pelkum *et al.* (2005). (b) Comparison of focal depths from the M1 and M2 seismic velocity models. M2 model was used in the Moho depth determination of Schulte-Pelkum *et al.* (2005) (shown).

located within the network (Fig. 2), but we also analyse four of the largest shallow earthquakes recorded by HIMNT in the southern Tibetan Plateau. Data preparation follows from Jost & Herrmann (1989). We removed trends and instrument responses from the data. Horizontal components are rotated into the transverse and radial orientations. We window each component of each station from the origin time to a group velocity of 1.0–2.0 km s⁻¹ depending on the source to station distance. We model the whole waveform for each component of each station filtered in the 5–100 s passbands. To reduce the dependence on origin time and earth model, the Green's functions and data are aligned with the *P*-wave first arrival before each inversion (Randall *et al.* 1995; Stich *et al.* 2003). The earthquakes in the deep (near-Moho) cluster under the High Himalaya and the southern Tibetan Plateau at $M_L < 4.0$ and epicentral distances <300 km generated seismograms containing sharp *P* and *S* phase onsets and weak surface waves. We filtered the deep events $M_L < 4$ from 5–30 s to preserve most of the body wave energy and the upper-crustal events $M_L > 4.0$ from 20–100 s to keep mostly the surface wave energy. We perform moment tensor inversions in a grid search over depth at 5 km increments for both M1 and M2 velocity models. The number of stations used for each earthquake varied from 4 to 14 depending on the available data, signal-to-noise and epicentral distances.

This moment tensor method assumes plane layers in the velocity model and station elevations at sea level even though stations positioned on the Tibetan Plateau were 3.0–4.0 km higher than ones positioned closer to the Himalayan arc. We subtract the average station elevations from the minimum misfit focal depth in order to

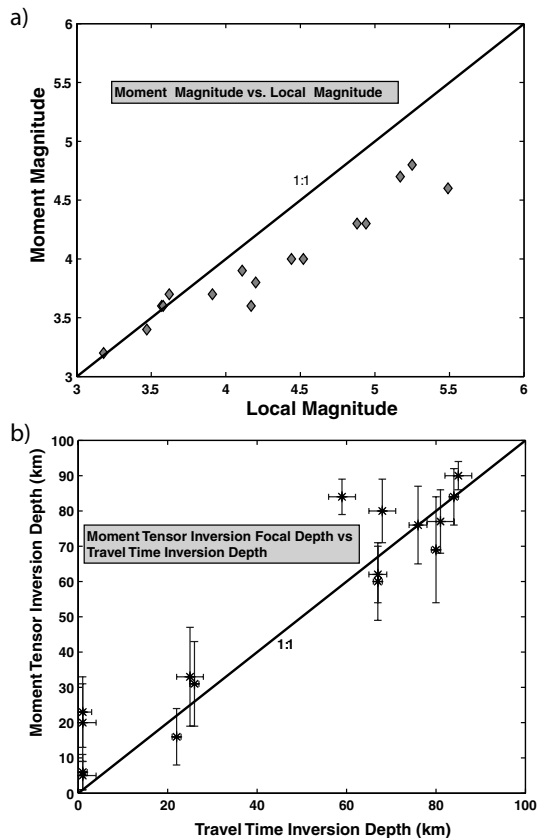


Figure 6. (a) Moment magnitude versus local magnitude (Monsalve *et al.* 2006) for Nos. 28–43 (Table 3). (b) Waveform inversion focal depths (Table 3) versus traveltimes inversion depths.

tabulate moment tensor focal depths, traveltime focal depths, and Moho depths all relative to a common datum of sea level (Table 3).

Moment tensor inversions for local earthquakes within the crust and upper mantle depend on the source depth. Misfit values can be highly dependent on focal depth for crustal earthquakes while fault plane solutions are often consistent around the minimum misfit depth (Sipkin 1982). For some earthquakes, we found that a source depth difference of 10 km can increase or decrease the amplitudes of the synthetic seismograms by 50 per cent. We perform solution sensitivity tests with different Earth velocity models. In general, we find that for the earthquakes near the Moho the fault plane solutions do not vary significantly with Earth velocity model used, but that the best fit focal depths increase in depth with increasing model Moho depths and shallow with decreasing model Moho depths.

We seek robust solutions with a clear and sharp minimum misfit over depth and a similar focal mechanism (Sipkin 1982). Solution and depth uncertainties are assigned by calculating the mean and standard deviations of all solutions with least squares misfit within 0.10 of the global minimum (Table 3). This method estimates focal depth error based upon the width of the misfit versus depth curves and is not a measure of the intrinsic errors in the inversion. We believe this range takes into account lateral heterogeneity and the range of solutions from velocity models M1 and M2. Using a range of 0.05 of the global minimum (Zhu & Helmberger 1996) reduces the standard error of the focal depths by ~5–7 km.

4.3 First motion check

We cross check the focal mechanism nodal planes from moment tensor inversions with first motion polarities. First motion polarities and take-off angles calculated using the traveltime hypocentral depths and the M1 velocity model are plotted on a lower hemisphere projection. For the first motion analysis we supplement the broadband data with seismograms from the short period vertical component network of the National Seismological Centre of the Department of Mines and Geology of Nepal (Pandey *et al.* 1999). We choose first motion polarities on the raw waveform without removing the instrument response. The number of stations with unambiguous first arrival polarities varies from earthquake to earthquake. For example, some earthquakes with poor ray coverage for the moment tensor inversion had twice the number of stations for the first motion determinations. Other events had six to ten stations with good quality signal for the moment tensor inversion, but had noisy or emergent first motion arrivals.

5 RESULTS

We use *P*- and *T*-axes orientations as approximations of the compressive strain orientations (Kostrov 1974; Frohlich & Apperson 1992) to estimate deformation processes (Tables 1–3). We show minimum misfit depths from both M1 and M2 velocity models (Fig. 5) and use the depth associated with the minimum misfit in our comparisons to previous published solutions (Fig. 4). Fault plane solutions of earthquakes located below the Moho using the M1 model in the moment tensor inversion were also below the Moho using the M2 model, but misfits using M2 generally rose by 0.05–0.10 and focal depths deepened by 5–20 km (Fig. 5). The fault plane solutions generally do not change between velocity models M1 and M2. Comparison of M_w determined from the moment tensor inversion to M_L determined from the amplitudes of the local seismograms with magnitude <4.0 while the local magnitudes are consistently

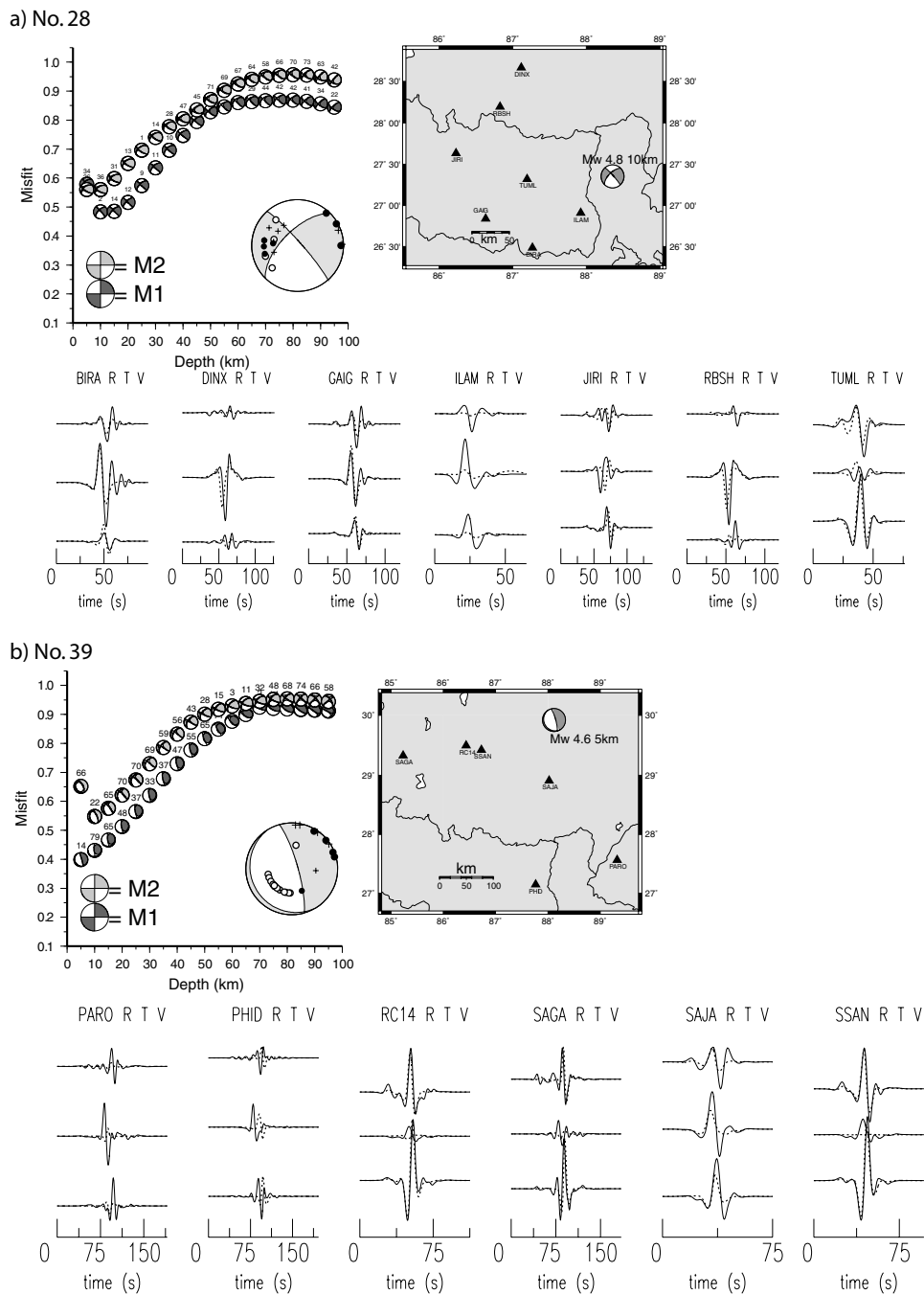


Figure 7. Summary solutions for earthquakes with focal depths <20 km. Focal depths are relative to station elevation. Top left panel shows the misfit versus depth curves for models M1 and M2 and first motion polarity points plotted on the best double-couple moment tensor solution. Numbers above each focal mechanism denote the non-double couple percentages for the solution at the associated depth. Map shows stations used in the inversion and event epicentre. Bottom panel shows synthetic waveforms (dashed line) and observed waveforms (solid) at the global minimum misfit as denoted in the top left panel for the Radial (R), Transverse (T) and Vertical (V) components. On the first motion plots, black dots are compression first arrivals, white circles are dilatational first arrivals, and ‘+’ indicates emergent or undetermined first motion arrivals. (a) Event No. 30 located in northeastern India indicated strike-slip at 15 km depth. (b) Event No. 41 indicated EW tension 5 km beneath the Tibetan Plateau.

greater than the moment magnitudes by ~0.5–0.7 magnitude units for events with magnitude >4.0 (Fig. 6a).

5.1 Focal depth comparisons

We compare the moment tensor derived depths to hypocentre depths determined from the NonLinLoc software, a probabilistic, non-

linear earthquake location in 3-D structures program (Lomax 2004). NonLinLoc uses a global optimization method where for each set of arrival times corresponding to one earthquake, the whole model space is searched, preventing convergence towards local minima. We consider these focal depths from traveltimes inversion (Monsalve *et al.* 2006) to be more accurate than the focal depths from moment tensor inversion.

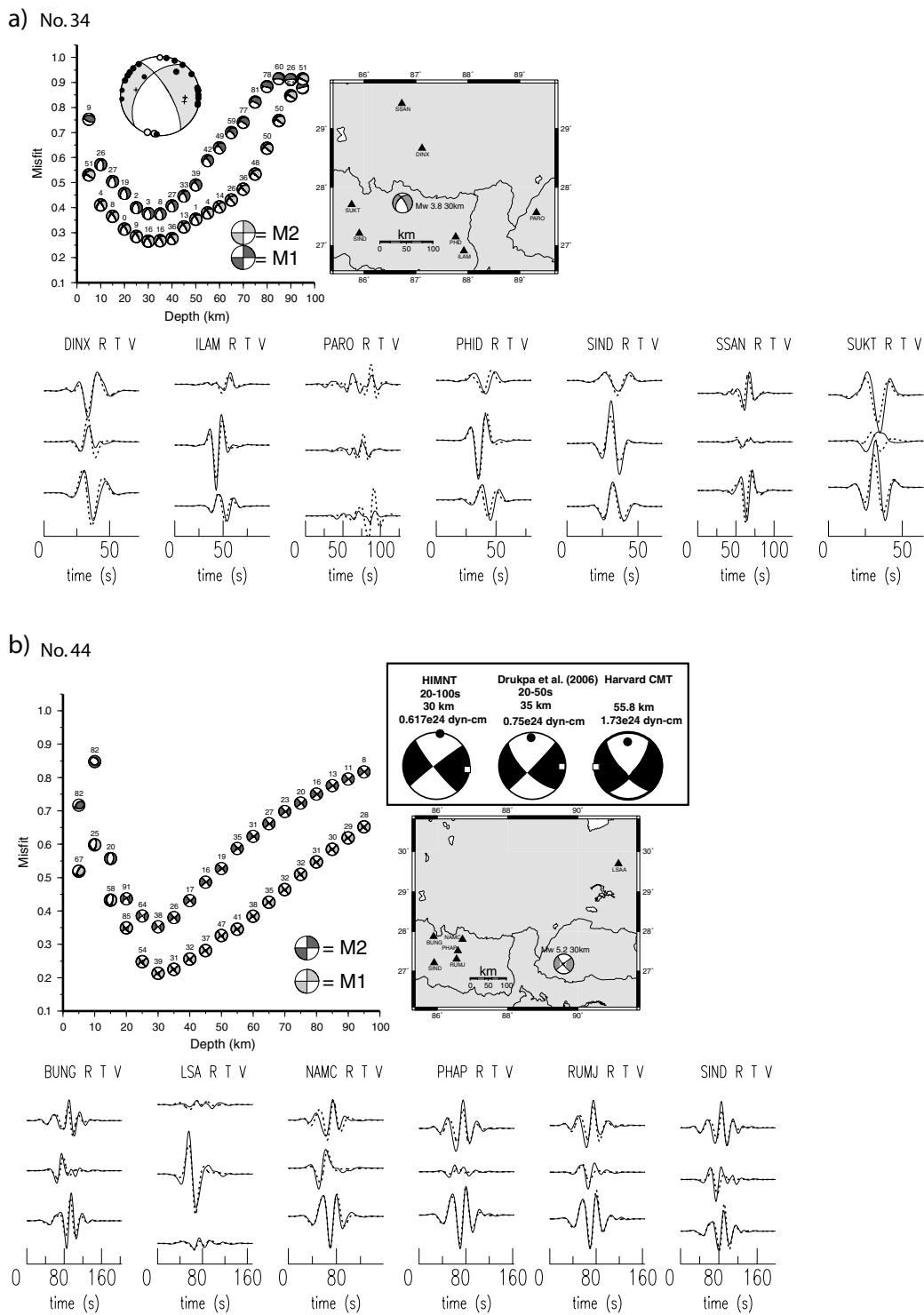


Figure 8. Summary solutions for two events in the 20–60 km focal depth range. Focal depths in the figure are relative to station elevation. Description as in Fig. 7. (a) No. 34 indicated normal faulting ~30 km below the Himalaya. (b) No. 44 indicated strike-slip in western Bhutan. The best solution has a focal depth of 30 km, a strike of 141.1°, dip of 82°, a rake of 176.6°, and a moment magnitude of 5.2 which is in agreement to the solution obtained by Drukpa *et al.* (2006).

Events 1–27 (Tables 1 and 2) are from previously published studies and are not included in the moment tensor versus traveltimes depth comparison. Events 28–44 are from this study and their corresponding information is given in Table 3. The mean moment tensor focal depths for 13 of these events are within the uncertainty bounds

of the traveltimes inversion depths. Three of our events have mean moment tensor focal depth outside the bounds of the traveltimes inversion depth by up to 17 km. These three events were all outside the HIMNT network, and we consider the moment tensor depths to be more robust for those events. Another earthquake, No. 44,

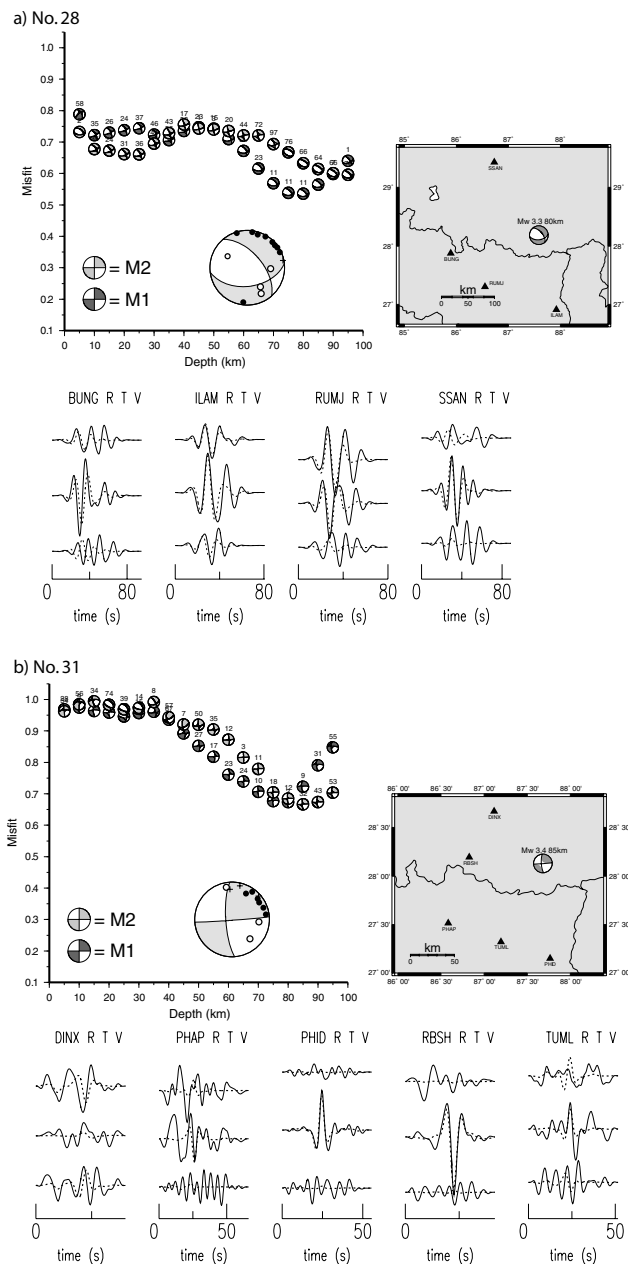


Figure 9. Summary solutions for six earthquakes with focal depths > 60 km (figure description same as in Fig. 7). (a) No. 28 indicated strike-slip with a large normal faulting component. The M1 model has a minimum misfit solution at 80 km relative to sea level, and M2, 95 km. Steeper dipping nodal planes would better match the first motion polarity points and would make the fault plane solution more similar to the other solutions > 60 km focal depth. Note the broad minimum misfit and consistent fault plane solutions from 55–90 km indicating that the moment tensor inversion method cannot resolve the depth well compared to the traveltimes inversion depth of 68 ± 3 km. We cannot resolve whether this is a lower crust or upper-mantle event. (b) No. 31 indicated strike-slip faulting at 75–90 km focal depth. The first motion polarities constrained one steeply dipping nodal plane supporting the strike-slip solution. (c) No. 37 indicated strike-slip faulting at 75 and 85 km minimum misfit depths under southern Nepal. Traveltimes inversion depth was 59 ± 3 km. This event had the greatest discrepancy between moment tensor and traveltimes determined depths, though both inversion methods place this event in the upper mantle. (d) No. 38 indicated normal faulting and almost pure double-couple slip at 65 km. This earthquake was most likely a double event. The sharp minimum at 65 km and a traveltimes inversion depth

was farther outside the network and was not located by traveltimes inversion.

5.2 Earthquakes 0–20 km depth

Four of the HIMNT events had depths less than 20 km (Nos. 30, 33, 40 and 41). No. 30 was a M_w 4.8 strike-slip event along the Himalayan arc in northeast India. The minimum misfit solution had 15 km focal depth with P -axis trending to the south and plunging 14° (Fig. 7a). Two of the shallow events we analysed were located beneath the southern Tibetan Plateau and had normal faulting with east–west extension (Nos. 33 and 41) (Fig. 7b). Somewhat noisy seismograms at the Nepal stations contributed to high misfit values, but the fault plane solutions remained consistent. These two events support the grouping of predominant normal faulting events near 31.1°N , 88.0°E , events Nos. 16–18 and 20–25 (Table 2).

For event No. 40 (see Appendix), use of both M1 and M2 models in the moment tensor inversion produce a strike-slip solution with minimum misfit at 20 km, but the traveltimes inversion depth is shallower. The first motion polarity plots suggest normal faulting, inconsistent with the moment tensor solution for this event. Moment tensor inversion with other Earth velocity models produce normal faulting from 5 to 10 km, but with higher misfit errors compared to the M1 and M2 models. Given that this event is well to the north of our network, we present this event as an interesting one warranting further study, and feel that it is not as well resolved as the in-network events.

5.3 Earthquakes 20 km $<$ depth $<$ 50 km

Four of HIMNT events had depths from 25 to 35 km (Nos. 29, 34, 36 and 44) and showed normal and strike-slip faulting. Event No. 29 showed east–west extension of the Tibetan Plateau. The fault plane solution is consistent over depth and velocity model, but the misfit/depth curve is very broad, indicating that focal depth is not well resolved. Event No. 36, a strike-slip earthquake with P -axis trending north–south, occurred on the Ganges Plain in northern Bangladesh. Misfit errors are smaller using the M2 model than the M1 model, suggesting that the seismic velocity and crustal thickness of the M2 model was more appropriate for northern Bangladesh. The first motion polarities are consistent with the minimum misfit moment tensor solution.

Event No. 34 was a normal faulting earthquake below the Main Himalayan Thrust beneath the Himalayan arc (Fig. 8a). A global minimum misfit in the 20–40 km depth range for both M1 and M2 models shows normal faulting solutions. The first motion polarity plot matches the moment tensor solution with all the dilatational polarities in the tension quadrants and 16 of 19 compressive polarities in the compressive quadrants.

Event No. 44 was one of the largest regional events recorded by the HIMNT network. It was a strike-slip earthquake along the Himalayan front in Bhutan, to the east of our network. Since it occurred after the end of the Bhutan broad-band deployment and

of 67 ± 2 implies an accurate focal depth. (e) No. 39 indicated strike-slip faulting at 95 km focal depth. The right quadrants of the focal sphere were constrained by the first motion points supporting the strike-slip solution. (f) No. 42 indicated consistent strike-slip faulting with a normal component for both models but the depth was not well resolved. Although the moment tensor depths fall within the range of the traveltimes inversion depth, 67 ± 1 km, we can only conclude that this event occurred near the Moho, either above or below it.

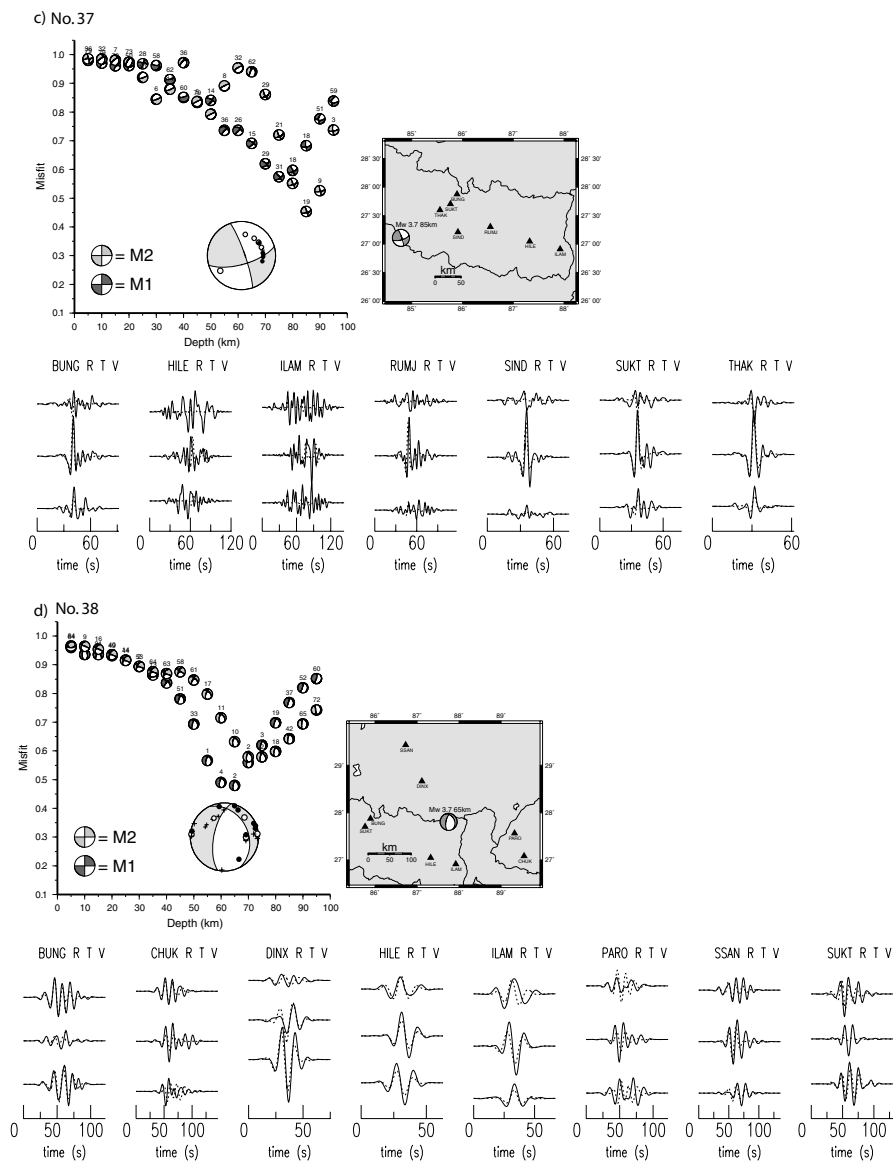


Figure 9. (Continued.)

near the end of the HIMNT deployment when only five stations were operating, we supplemented the moment tensor inversion with data from station LSA. It was the only event our network recorded for which the Harvard Centroid Moment Tensor catalogue also had a moment tensor solution for, making it an important event to compare methods. The minimum misfit moment tensor solution from our study showed a strike-slip earthquake at a depth of 35 ± 8 km (Fig. 8, Table 3) while Harvard CMT solution was also a strike-slip event but at a depth of 55.8 km. The event was also modelled as a strike-slip event at a depth of 35 km (Drukpa *et al.* 2006) while the EHB catalogue locates the hypocentre depth at 35 km (Engdahl *et al.* 1998). The fault plane solutions from this study, the Harvard CMT catalogue, and from Drukpa *et al.* (2006) are summarized in Fig. 8.

5.4 Earthquakes > 50 km

Eight of the HIMNT events had minimum misfit focal depths ≥ 60 km (Nos. 28, 31, 32, 35, 37, 38, 39 and 43) and one event had a minimum misfit focal depth of 55 km (No. 42) (Figs 3, 4 and

9). Seven of these deep continental events clustered under the High Himalaya within the HIMNT network, one occurred ~ 100 km west of the northern HIMNT stations, and one was ~ 100 km southwest of Kathmandu. With the exception of No. 38 which was a normal faulting event, these earthquakes showed strike slip faulting with some normal component on two of them (Nos. 28 and 42).

The event southwest of Kathmandu (No. 37) (Fig. 9c) was a strike-slip event at minimum misfit focal depth of 75 km for the M1 model, 85 km for M2, and 59 ± 3 km from the traveltime inversion using the NonLinLoc program. This event was one of three earthquakes where the traveltime inversion and moment tensor inversion depths differed by more than 10 km, and the event occurred outside of the HIMNT network. The narrow misfit error curve around the minimum at depths ≥ 75 km from the M1 model suggests that the moment tensor inversion depths were robust ones (Fig. 9c). The first motion comparison constrained only the east–west striking nodal plane due to the limited azimuthal coverage. Both the traveltime inversion depth and moment tensor inversion depths are greater than the 48–55 km Moho depth estimates for the northern India/Nepal

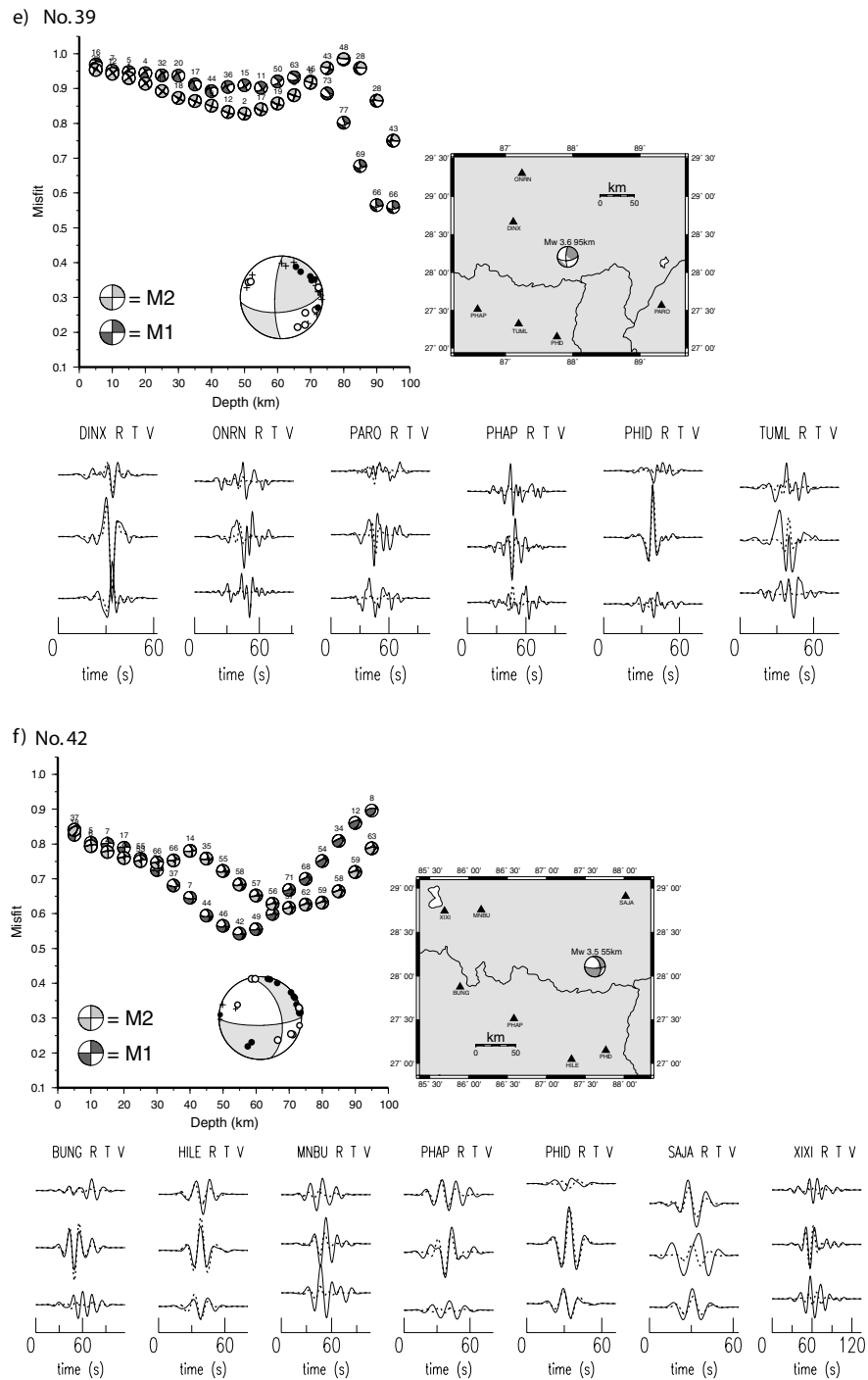


Figure 9. (Continued.)

crust (Pandey *et al.* 1995; Schulte-Pelkum *et al.* 2005; Mitra *et al.* 2005).

Moment tensor inversion for Event No. 38 (Fig. 9d) produced normal faulting at 65 km minimum misfit depth. This event appears to be a double event as two *P* phase arrivals ~ 5 s apart were observed at all stations independent of event to station distances. The second *P* arrival was the larger of the two while the first was barely visible at epicentral distances >250 km. Since the inversion method assumes a simple point source, we treated the second arrival as the main event and used the 10–20 s pass band to remove smaller amplitudes and high frequencies of the smaller event.

First motion polarities picked on the second subevent were problematic due to noise from the first event. This earthquake could be in the lower crust or in the upper mantle given the range of focal depths and the ± 5 km bounds on Moho depth (Schulte-Pelkum *et al.* 2005).

5.4.1 Strike-slip earthquakes

The seven deep earthquakes under the High Himalaya and the southern Tibetan Plateau (Nos. 28, 31, 32, 35, 39, 42 and 43) were

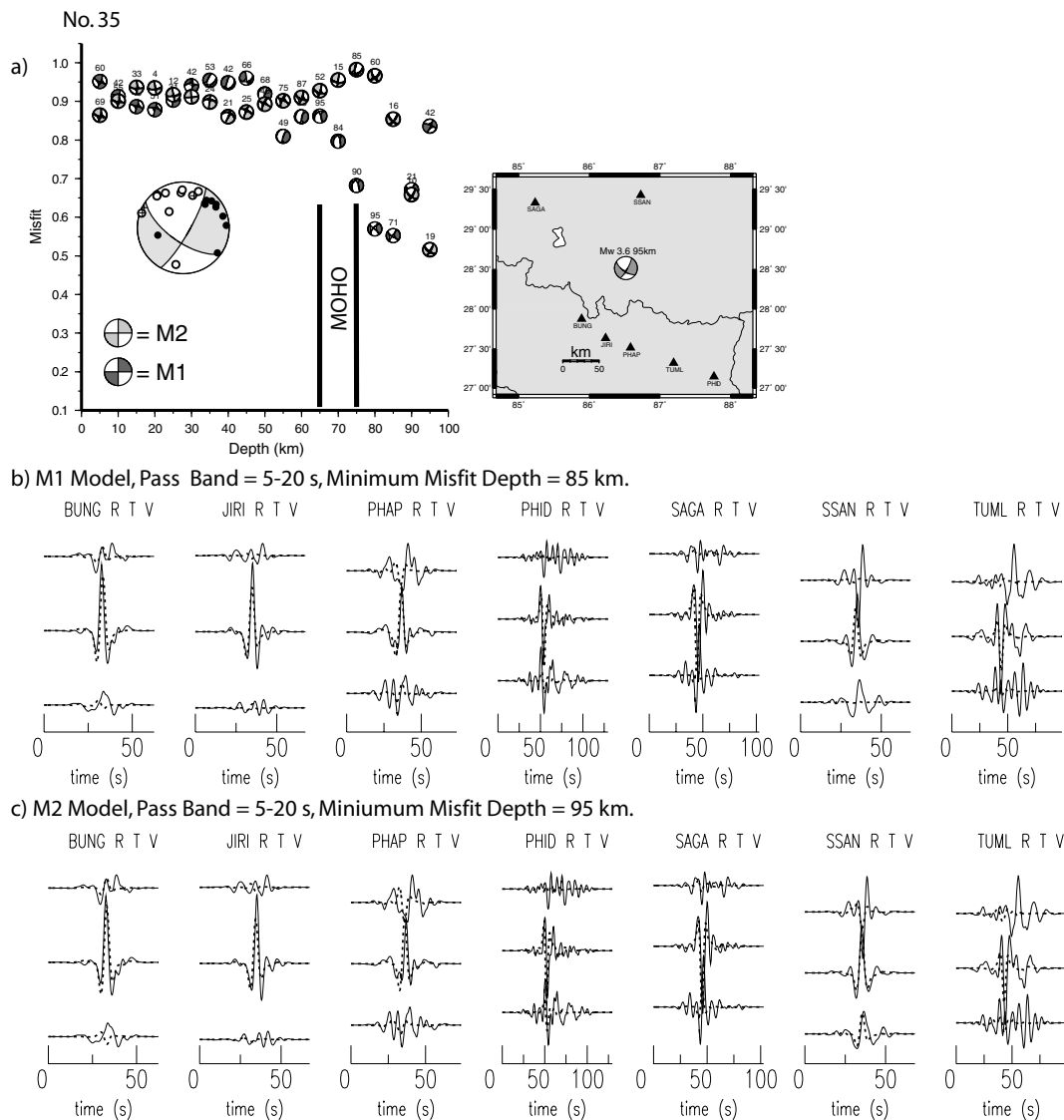


Figure 10. Summary solution for No. 35, located under the Himalaya at 28.5°N , 86.5°E , 84 ± 1 km depth by travelt ime inversion. Minimum misfits occur at 83 km depth for the M1 model, 93 km depth for the M2 model, and average moment tensor focal depth of 84 ± 5 km relative to sea level (Table 3). Synthetic seismograms (dotted) are plotted on top of observed seismograms (solid) for the minimum misfits of both models. The solution relied on the larger amplitude transverse components while noise on the lower amplitude radial and vertical components accounted for most of the misfit. The sharp minimum from both models, the agreement with travelt ime inversion depth, 84 ± 1 km, and the first motion points supporting a strike-slip solution accurately show that shear brittle deformation can occur in the continental upper mantle.

dominantly strike-slip with P -axes trending NW–SE to NE–SW. P -axis plunge was near horizontal for four of these earthquakes (4.5° , 8.6° , 10.2° and 25.9°) and at $\sim 40^{\circ}$ – 57° for three. From the travelt ime inversion depths (Monsalve *et al.* 2006) and their correlation to the depths determined in this study (Fig. 6 and Table 3), we conclude that four of these earthquakes were most likely sub-Moho events (Nos. 31, 35, 39 and 43) while three of these earthquakes could be either in the lower crust or upper mantle given the errors (Nos. 28, 32 and 42).

Event No. 35 was located by travelt ime inversion under the Himalaya at 28.5°N , 86.5°E , 84 ± 1 km depth, and at minimum misfit focal depths of 85 and 95 km through moment tensor inversions with models M1 and M2 (Fig. 10). Large transverse amplitudes and small radial and vertical amplitudes characterized the seismograms from stations at epicentral distances 47–194 km. The P and S phases in the synthetic seismograms were best-fitting on

the transverse components constraining the strike-slip component of the earthquake. The first motion polarities, save one, were consistent with the moment tensor focal mechanism solution. Synthetic and observed waveform comparisons show that the best focal depth for this earthquake is in the 80–95 km range (Fig. 11).

6 DISCUSSION

Moment tensor solutions from this study are combined with previously published results to arrive at a more complete picture of Himalayan deformation (Figs 2 and 3). The seismic zones are comprised of varying faulting mechanisms showing P and T -axis orientation shifts with depth (Fig. 12). In particular, the plunge of the P -axes for events beneath the southern Tibetan Plateau shift from vertical for events with focal depths < 60 km to horizontal for events

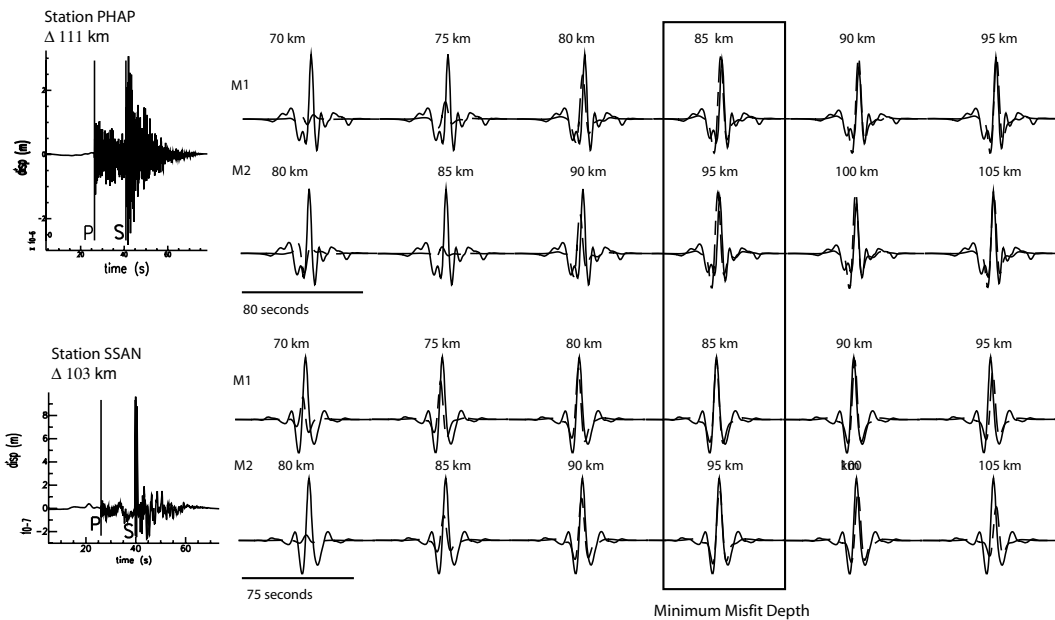


Figure 11. To the left, synthetic (dashed) versus observed (solid) transverse component seismograms filtered 5–20 s for No. 35 are plotted for a range of depths for stations PHAP and SSAN to observe how the best fitting waveforms occurred at depths below the Moho. Under the Himalaya, the Moho depth estimates were 60–70 km (Yuan *et al.* 1997; Mitra *et al.* 2005; Schulte-Pelkum *et al.* 2005). The best fit to the observed seismograms occurred at 85 and 95 km. To the right, the unfiltered transverse component seismograms show sharp *P* and *S* arrivals and little surface wave energy which is characteristic of sub-Moho events in this study and from Zhu & Helmberger (1996).

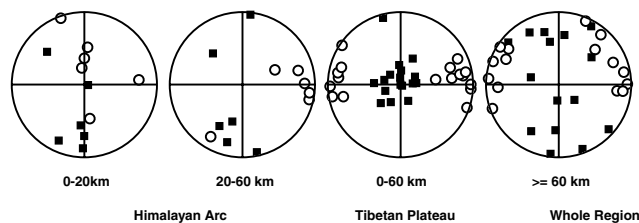


Figure 12. Lower hemisphere projections of *T*-axes (open circles) and *P*-axes (closed squares) of focal mechanisms from Fig. 3 by region and depth. From left to right: Upper-crustal earthquakes <20 km depth under the Himalayan arc south of 28.5°N represent NS shortening by the shallow plunging *P*-axes and steeply dipping *T*-axes. Earthquakes at depths 20–60 km beneath the Himalayan arc show shallow plunging *P*-axes and one *P*-axis plunging at >45°. Shallow plunging *T*-axes characterize EW extension. Upper-crustal earthquakes at depths <60 km under the southern Tibetan Plateau show vertical *P*-axes and E–W trending *T*-axes. These events imply extension parallel and oblique to the Himalayan arc. Earthquakes at depths >60 km beneath the entire region show NNW–SSE to NNE–SSW trending *P*-axes with shallow plunging *T*-axes. Strike-slip faulting and EW extension accommodate the deformation near and below the Moho.

with focal depths >60 km, with the exception of one deep normal faulting earthquake (No. 4 Fig. 3 and Table 1).

Under the southern Tibetan Plateau near 30°N, NS striking normal faults cluster in the upper crust suggestive of active localized east–west extension (Molnar & Lyon-Caen 1989) (Figs 2 and 9d). In the Himalayan arc at depths of 0–20 km, thrust events with $M_w > 5.0$ (Nos. 1, 3, 12 and 27) indicate active underthrusting by the India Shield (Molnar & Lyon-Caen 1989). The strike-slip earthquakes with focal depths <40 km that we find in eastern Nepal and Bhutan are consistent with a conjugate system of strike-slip faulting that accompanies the formation of grabens in the Himalaya and southern

Tibetan Plateau (Dasgupta *et al.* 1987) and with midcrustal transcurrent deformation (Drukpa *et al.* 2006).

6.1 Lower crustal/upper-mantle earthquakes

From Nepal to the southern Tibetan Plateau, strike-slip faulting with *P*-axes trending NNW–SSE to NNE–SSW and *T*-axes trending EW reflect vertical plane shear at and below the Moho (Figs 3 and 9). The focal mechanisms of these earthquakes are similar to those from previous studies (Nos. 2, 7, 9, 11 and 26) and suggest that strike-slip faulting is the dominant deformation style near the Moho. Because of the proximity to the Himalayan collision zone, these strike-slip earthquakes suggest the India lithosphere at depths 70–100 km below the High Himalaya and southern Tibetan Plateau must be involved in accommodating convergent strains (Baranowski *et al.* 1984; Ni & Barazangi 1984; Molnar & Lyon-Caen 1989).

6.2 Re-examining the focal depths from previous studies

We recalculated the focal depths of events 2 and 4 based on the pP–P times at World Wide Standard Seismographic Network (WWSSN) stations (Chen *et al.* 1981; Molnar & Chen 1983). The published focal depth for No. 2 was 85 ± 10 km (Molnar & Chen 1983) and for No. 4 was 90 ± 10 km (Chen *et al.* 1981), both assuming a 70 km Moho depth. We utilized the TauP Toolkit (Crotwell *et al.* 1999) with a number of different earth models including that of Molnar and Chen (1983), Cotte *et al.* (1999), Mitra *et al.* (2005), and the M2 model to recalculate focal depths for events Nos. 2 and 4 (Table 5). Moho depths have been reported to be as deep as 80–88 km near 29.9°N (Yuan *et al.* 1997; Mitra *et al.* 2005) which supports the case that these two events ruptured in the crust (Maggi *et al.* 2000b; Jackson 2002b, Jackson *et al.* 2004; Mitra *et al.* 2005). However, our analysis places event No. 4 in the upper mantle

Table 5. Recalculated topography corrected focal depths from pP–P times (Chen *et al.* 1981; Molnar & Chen 1983) using different models of the Tibetan Plateau (Topography $V_P = 5.5 \text{ km s}^{-1}$ and height = 4 km).

Event #2 8/1/1973 WWSSN Station	Molnar & Chen (1983) pP–P (s)	70 km Moho Molnar & Chen (1983)		70 km Moho Cotte <i>et al.</i> (1999)		75 km Moho Schulte-Pelkum <i>et al.</i> (2005)		80 km Moho Mitra <i>et al.</i> (2005)		88 km Moho Mitra <i>et al.</i> (2005)	
		Depth (km)	±	Depth (km)	±	Depth (km)	±	Depth (km)	±	Depth (km)	±
EIL	25 ± 1.0	82	5	86	5	86	5	83	5	79	5
COL	26.5 ± 0.5	82	3	86	5	85	5	83	3	85	3
KOD	24 ± 0.5	92	3	102	3	101	3	98	3	96	3
KTG	26 ± 2.0	82	10	85	10	84	10	82	10	84	10
NUR	24.5 ± 0.5	78	3	82	3	82	3	79	3	81	3
UME	25 ± 1.0	80	5	84	5	83	5	81	5	83	5
	Average ^a	84	6	89	9	89	9	86	8	86	7
Event #4 9/14/1976 WWSSN Station	Chen <i>et al.</i> (1981) pP–P (s)	Depth (km)	±	Depth (km)	±	Depth (km)	±	Depth (km)	±	Depth (km)	±
ATH	26 ± 2	85	10	89	10	88	10	86	10	87	10
COL	28 ± .5	89	2	93	3	92	3	90	2	91	2
JER	27 ± 1	92	6	97	5	96	5	94	5	94	6
MAL	27 ± 1	84	5	88	5	87	5	85	5	86	5
STU	27 ± .5	88	3	91	3	91	3	89	3	89	3
TRI	26 ± 1	83	5	87	5	87	5	85	5	86	5
	Average ^d	88	3	92	3	91	3	89	3	90	2

^aWeighted according to $1/(\text{pP–P uncertainties})^2$.

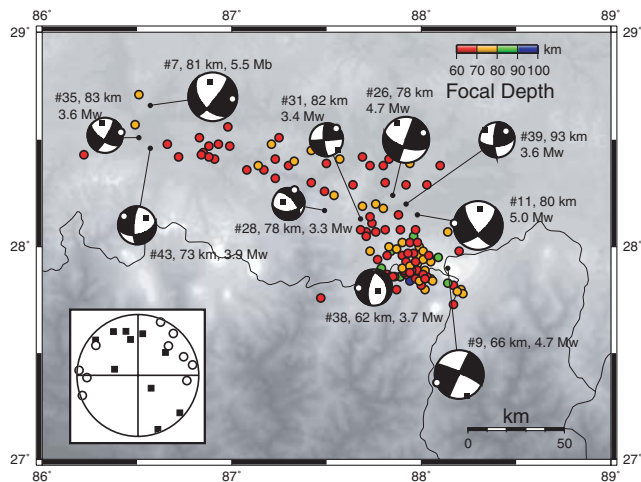


Figure 13. Focal mechanisms under the High Himalaya and the southern edge of the Tibetan Plateau show strike-slip faulting and one normal faulting earthquake (No. 38). The inset is a lower hemisphere plot similar to Fig. 13 showing mostly NW–SE P -axis orientations. Circles are 60–100 km depth hypocenters from Monsalve *et al.* (2006).

for all velocity models examined, and event 2 in the upper mantle in all cases except when using the model with an 88 km Moho (Table 5). The 88 km Moho velocity model contains a seismically slow upper mantle which is not consistent with the mantle speeds of $8.1\text{--}8.4 \text{ km s}^{-1}$ observed under the southern Tibetan Plateau (McNamara *et al.* 1995, 1997; Monsalve *et al.* 2006).

Next, we considered whether events 9 and 11 occurred in the upper mantle as reported by Zhu & Helmberger (1996) (Table 1). Jackson (2002a) claimed that these events cannot conclusively be below the Moho because lower crustal discontinuities 15–20 km above the Moho (Yuan *et al.* 1997) would generate the same effect as a crust–mantle discontinuity in waveform modelling. These two events occurred at similar focal depths and contained similar strike-slip fault plane solutions as the earthquake cluster from our study (Figs 3, 4 and 12). In addition, the transverse components for

these two events contain sharp S wave onsets (Zhu & Helmberger 1996) similar to the S wave onsets we observed in the transverse seismograms from our study. Based upon similarity to our possible subcrustal events Nos. 28, 31, 32, 35, 39, 42 and 43, we conclude events Nos. 9 and 11 also occurred at similar depths (Zhu & Helmberger 1996; Fig. 4).

6.3 Seismotectonic interpretation

The earthquakes that we observe signify that brittle deformation occurred near the Moho beneath the Himalaya and the southern Tibetan Plateau (Figs 12–14). Large magnitude shallow thrust earthquakes above the Main Himalayan Thrust accommodate N–S shortening in the upper India crust (Molnar & Lyon-Caen 1989) while possible N–S extension (No. 5) accommodates upper-crustal flexure of the India crust (Ni & Barazangi 1984). Below this extension, thrust or reverse earthquakes like the Udayapur event (No. 8) accommodates contraction in the India lower crust or upper mantle (Chen & Kao 1996). One earthquake (No. 34) below the microearthquakes along the Himalayan arc suggests possible E–W extension accommodating segmentation of the Main Himalayan Thrust near 87°E (Pandey *et al.* 1999) in the India crustor collapse under load from the Himalaya. If normal faulting is characteristic along the Himalayan arc, any estimation of crustal shortening has to be considered within the context of extension parallel to the convergent front.

On the southern Tibetan Plateau 200–300 km north from the Himalayan seismicity, shallow N–S striking normal faulting accommodates E–W extension and possible gravitational collapse. Beneath the entire region at depths $\sim >60$ km, strike slip faulting with N–S trending P -axes appears to be the main mode of deformation. The strike-slip cluster under the High Himalaya contains two patterns: one along 200 km of the Himalayan arc with depths from 60 to 80 km, and the other clustering at 28°N , and ranging from 60 to 100 km focal depth. Strike-slip faulting dominates both groups with the exception of one normal faulting event.

The epicentral pattern of earthquakes under the High Himalaya at depths >60 km seen in this study is also seen with earthquakes located by the National Seismological Network of Nepal from 1994

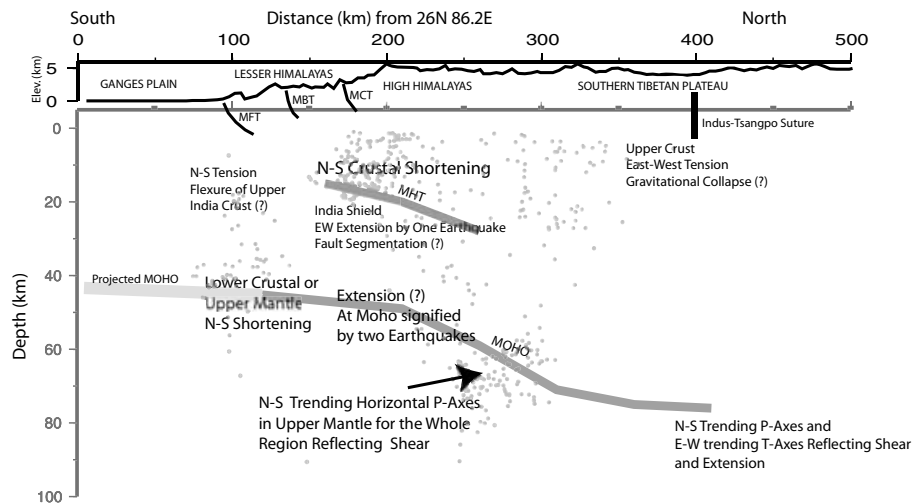


Figure 14. Seismotectonic interpretation from the earthquake mechanisms in Tables 1–3 in a 500 km cross section from 26°N 86.2°E at azimuth 018°. The figure includes the seismicity from Fig. 2, the locations of the Main Himalayan Thrust (MHT, dark grey), the Moho (dark grey) from Schulte-Pelkum *et al.* (2005) and the approximate location of the Indus-Tsangpo Suture. N–S crustal shortening under the High Himalaya and EW extension in the southern Tibetan Plateau (Molnar & Lyon-Caen 1989), NS tension of the upper Indian Shield south of the Main Frontal Thrust and lower crustal and upper mantle shortening of India Plate (Ni & Barzangi 1984; Chen & Kao 1996). Focal mechanisms indicate shear in the lower crust and upper mantle beneath the High Himalaya. MFT, Main Frontal Thrust; MBT, Main Boundary Thrust and MCT, Main Central Thrust.

May to 1998 January (Pandey *et al.* 1999). Assuming that these earthquakes were at depths similar to the cluster detected by the HIMNT network, earthquakes near the Moho under the High Himalaya are common. Chen & Yang (2004) argue that earthquakes at this depth range in this region are unrelated to subduction processes due the faulting similarities to the upper Tibetan crust mechanisms and faulting differences to earthquakes along the Himalayan front. However, we have shown that fault plane solutions for the cluster of events at depths >60 km have horizontal *P*-axes nearly parallel to the convergence direction and parallel to the *P*-axis orientations of shallow thrust earthquakes. These *P*-axis orientations suggest a correlation between the convergent process and the earthquakes at Moho depths.

7 CONCLUSION

The focal mechanisms calculated from local and regional earthquakes in eastern Nepal indicate north–south trending *P*-axis orientations at depths >60 km. Although no earthquake analysed for a fault plane solution from the HIMNT data set showed thrusting <20 km depth characteristic of India underthrusting Asia, the strike-slip events from this study show *P*-axes trending parallel to the direction of convergence. The solutions for the upper crustal events in the southern Tibetan Plateau showed east–west tension, further indication of gravitational collapse as the Tibetan Plateau is being stretched apart. Under the Himalaya at the mid crust, east–west tension is also present accommodating possible active extension of the India crust below the Main Himalayan Thrust. The *P*-axis orientation for events on the Himalayan front to the southern Tibetan Plateau shifts from a combination of vertical orientations at focal depths <60 km to just horizontal at focal depths >60 km. This shift could be indicative of body forces dominating in the upper crust to plate forces dominating at deeper depths. We infer that strike-slip faulting is the primary mode of deformation clustering in the vicinity of the Moho and nearly parallel to the Himalayan arc.

ACKNOWLEDGMENTS

We thank George Randall for enlightening discussions on our moment tensor solutions, Charles Ammon for making the moment tensor codes available for use, Arthur Rodgers for organizational suggestions to get this study started, Peter Molnar for critically reading drafts of this manuscript, and the IRIS Consortium for providing the instruments and data-processing assistance. We especially thank the National Seismic Center of the Department of Mines and Geology Nepal for assistance with the HIMNT deployment and for providing the data used for the first motion study. F. Blume, R. Bendick, D. Tiwari, G. Chitrakar, B. Chaudari, U. Gautam, P. Shresta, B. Kaffle, S. Rajure, M. R. Pandey and N. R. Sthapit provided invaluable assistance related to the HIMNT field experiment. We thank Aaron Velasco and Vicki Lee Gee for providing the data from the Bhutan broad-band experiment. Maps and plots were generated using the Generic Mapping Tool (Wessel & Smith 1991) and Matlab by the MathWorks, Inc.

REFERENCES

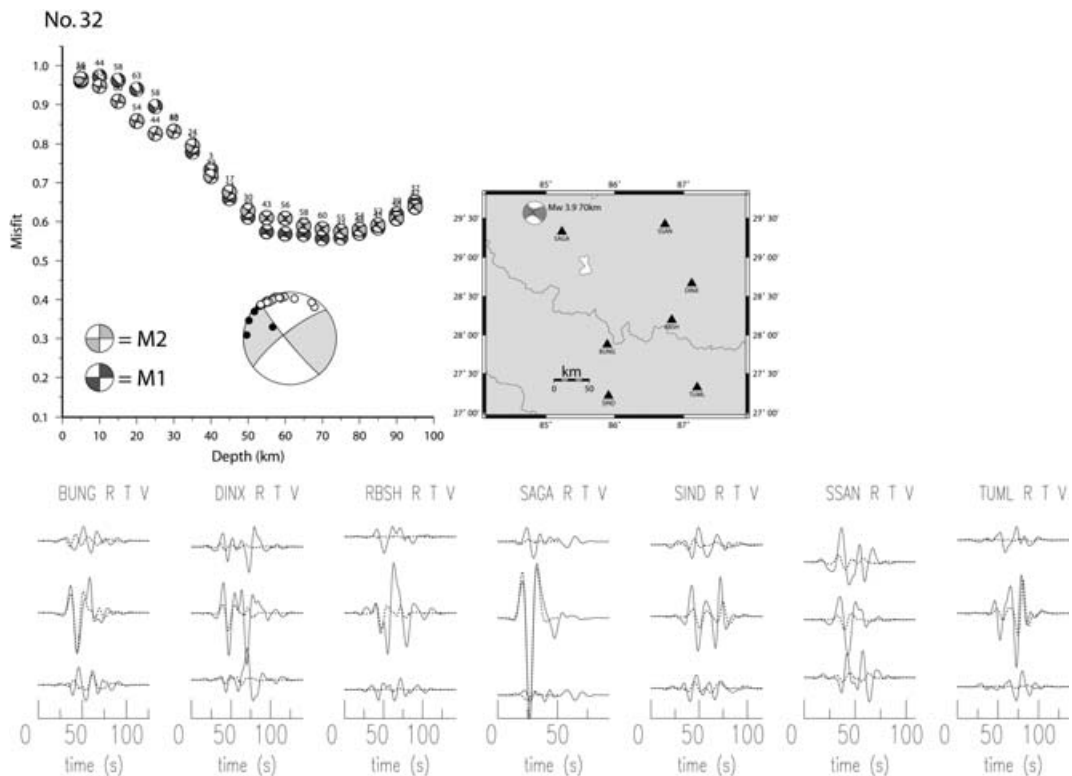
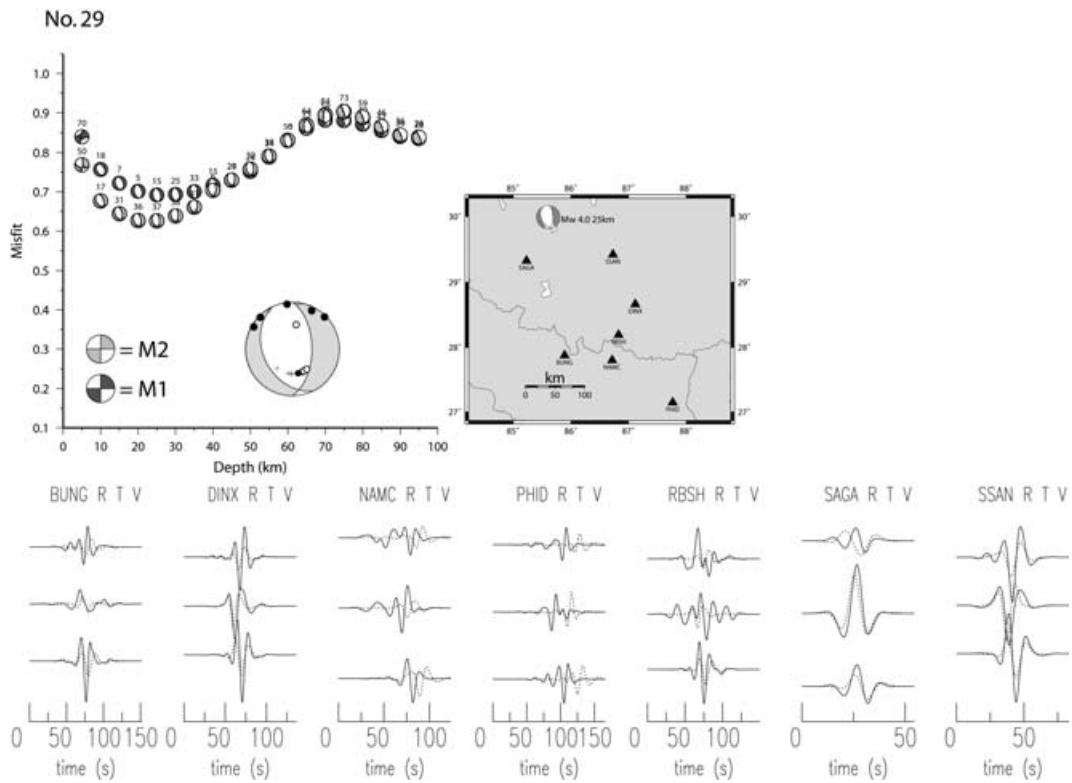
- Ammon, C.J. & Randall, G.E., 1994. mtinv, Deviatoric moment tensor inversion, <http://eqseis.geosc.psu.edu/~cammon/HTML/MTinvDocs/mtinv01.html>.
- Armijo, R., Tapponnier, P., Mercier, J.L. & Han, T.L., 1986. Quaternary extension in Southern Tibet – Field observations and tectonic implications, *J. Geophys. Res.-Solid Earth Planets*, **91**, 13 803–13 872.
- Baranowski, J., Armbruster, J., Seeber, L. & Molnar, P., 1984. Focal depths and fault plane solutions of earthquakes and active tectonics of the Himalaya, *J. Geophys. Res.*, **89**, 6918–6928.
- Bilham, R., *et al.*, 1997. GPS measurements of present-day convergence across the Nepal Himalaya, *Nature*, **386**, 61–64.
- Bollinger, L., Avouac, J.P., Cattin, R. & Pandey, M.R., 2004. Stress buildup in the Himalaya, *J. Geophys. Res.-Solid Earth*, **109**, B11405.
- Cattin, R. & Avouac, J.P., 2000. Modeling mountain building and the seismic cycle in the Himalaya of Nepal, *J. Geophys. Res.-Solid Earth*, **105**, 13389–13407.

- Chen, W.P. & Kao, H., 1996. Seismotectonics of Asia: Some recent progress, in *The Tectonic Evolution of Asia*, pp 37–62, eds A. Yin & M. Harrison, Cambridge University Press, Cambridge.
- Chen, W.P. & Molnar, P., 1983. Focal depths of intracontinental and intraplate earthquakes and their implications for the thermal and mechanical properties of the lithosphere, *J. Geophys. Res.*, **88**, 4183–4214.
- Chen, W.P., Nabelek, J.L., Fitch, T.J. & Molnar, P., 1981. An intermediate depth earthquake beneath Tibet—source characteristics of the event of September 14, 1976, *J. Geophys. Res.*, **86**, 2863–2876.
- Chen, W.P. & Yang, Z.H., 2004. Earthquakes beneath the Himalayas and Tibet: evidence for strong lithospheric mantle, *Science*, **304**, 1949–1952.
- Cotte, N., Pedersen, H., Campillo, M., Mars, J., Ni, J.F., Kind, R., Sandvol, E. & Zhao, W., 1999. Determination of the crustal structure in southern Tibet by dispersion and amplitude analysis of Rayleigh waves, *Geophys. J. Int.*, **138**, 809–819.
- Crotwell, H.P., Owens, T.J. & Ritsema, J., 1999. The TauP Toolkit: Flexible seismic travel-time and raypath utilities, *Seismol. Res. Lett.*, **70**, 154–160.
- Dasgupta, S., Mukhopadhyay, M. & Nandy, D.R., 1987. Active transverse features in the central portion of the Himalaya, *Tectonophysics*, **136**, 255–264.
- Drukpa, D., Velasco, A.A. & Doser, D.I., 2006. Seismicity in the Kingdom of Bhutan (1937–2003): evidence for crustal transcurrent deformation, *J. Geophys. Res.-Solid Earth*, **111**, B06301.
- Engdahl, E.R., Van Der Hilst, R. & Buland, R., 1998. Global teleseismic earthquake relocation with improved travel times and procedures for depth determination, *Bull. Seismol. Soc. Am.*, **88**, 722–743.
- Feldl, N., 2005. Crustal deformation across the Himalaya of eastern and central Nepal, *Masters thesis*. University of Colorado at Boulder, Boulder.
- Frohlich, C. & Apperson, K.D., 1992. Earthquake focal mechanisms, moment tensors, and the consistency of seismic activity near plate boundaries, *Tectonics*, **11**, 279–296.
- Harvard University Department of Geological Sciences, 2005. *Centroid Moment Tensor Catalog*, www.seismology.harvard.edu/CMTsearch.html
- Ichinose, G.A., Anderson, J.G., Smith, K.D. & Zeng, Y.H., 2003. Source parameters of eastern California and western Nevada earthquakes from regional moment tensor inversion, *Bull. Seismol. Soc. Am.*, **93**, 61–84.
- Jackson, J., 2002a. Faulting, flow, and the strength of the continental lithosphere, *Int. Geol. Rev.*, **44**, 39–61.
- Jackson, J., 2002b. Strength of the continental lithosphere: time to abandon the jelly sandwich?, *GSA Today*, **12**, 4–10.
- Jackson, J.A., Austrheim, H., McKenzie, D. & Priestley, K., 2004. Metastability, mechanical strength, and the support of mountain belts, *Geology*, **32**, 625–628.
- Jost, M.L. & Herrmann, R.B., 1989. A student's guide to and review of moment tensors, *Seismol. Res. Lett.*, **60**, 37–56.
- Kayal, J.R., 2001. Microearthquake activity in some parts of the Himalaya and the tectonic model, *Tectonophysics*, **339**, 331–351.
- Kostrov, V.V., 1974. Seismic moment and energy of earthquakes, and seismic flow of rock, *Isv. Acad. Sci. USSR Phys. Solid Earth* (translated by F. Goodspeed), **1**, 23–40.
- Kumar, B., 1998. Aftershock distribution and focal mechanism of Sarshin earthquake, individual studies by participants at the *Int. Inst. Seismol. Earthquake Eng.*, **34**, 117–127.
- Lave, J. & Avouac, J.P., 2000. Active folding of fluvial terraces across the Siwaliks Hills, Himalayas of central Nepal, *J. Geophys. Res.-Solid Earth*, **105**, 5735–5770.
- Lomax, A., 2004. *NonLinLoc version 3.03, Probabilistic, Non-Linear, Global-Search Earthquake Location in 3D Media*, Anthony Lomax Scientific Software.
- Maggi, A., Jackson, J.A., McKenzie, D. & Priestley, K., 2000a. Earthquake focal depths, effective elastic thickness, and the strength of the continental lithosphere, *Geology*, **28**, 495–498.
- Maggi, A., Jackson, J.A., Priestley, K. & Baker, C., 2000b. A re-assessment of focal depth distributions in southern Iran, the Tien Shan and northern India: do earthquakes really occur in the continental mantle?, *Geophys. J. Int.*, **143**, 629–661.
- McKenzie, D., Jackson, J. & Priestley, K., 2005. Thermal structure of oceanic and continental lithosphere, *Earth Planet. Sci. Lett.*, **233**, 337–349.
- McNamara, D.E., Owens, T.J. & Walter, W.R., 1995. Observations of regional phase propagation across the Tibetan plateau, *J. Geophys. Res.-Solid Earth*, **100**, 22 215–22 229.
- McNamara, D.E., Walter, W.R., Owens, T.J. & Ammon, C.J., 1997. Upper mantle velocity structure beneath the Tibetan Plateau from Pn travel time tomography, *J. Geophys. Res.-Solid Earth*, **102**, 493–505.
- Mitra, S., Priestley, K., Bhattacharyya, A.K. & Gaur, V.K., 2005. Crustal structure and earthquake focal depths beneath northeastern India and southern Tibet, *Geophys. J. Int.*, **160**, 227–248.
- Molnar, P. & Chen, W.P., 1983. Focal depths and fault plane solutions of earthquakes under the Tibetan Plateau, *J. Geophys. Res.*, **88**, 1180–1196.
- Molnar, P. & Lyon-Caen, H., 1989. Fault plane solutions of earthquakes and active tectonics of the Tibetan Plateau and its margins, *Geophys. J. Int.*, **99**, 123–153.
- Monsalve, G., Sheehan, A., Schulte-Pelkum, V., Rajaure, S. & Wu, F., 2006. Seismicity and one-dimensional velocity structure of the Himalayan collision zone: Earthquake in the crust and upper mantle, *J. Geophys. Res.-Solid Earth*, **111**, B10301.
- Ni, J. & Barazangi, M., 1984. Seismotectonics of the Himalayan collision zone—geometry of the underthrusting Indian plate beneath the Himalaya, *J. Geophys. Res.*, **89**, 1147–1163.
- Pandey, M.R., Tandukar, R.P., Avouac, J.P., Lave, J. & Massot, J.P., 1995. Interseismic strain accumulation on the Himalayan crustal ramp (Nepal), *Geophys. Res. Lett.*, **22**, 751–754.
- Pandey, M.R., Tandukar, R.P., Avouac, J.P., Vergne, J. & Heritier, T., 1999. Seismotectonics of the Nepal Himalaya from a local seismic network, *J. Asian Earth Sci.*, **17**, 703–712.
- Randall, G.E., 1994. Efficient calculation of complete differential seismograms for laterally homogenous earth models, *Geophys. J. Int.*, **118**, 245–254.
- Randall, G.E., Ammon, C.J. & Owens, T.J., 1995. Moment tensor estimation using regional seismograms from a Tibetan Plateau portable network deployment, *Geophys. Res. Lett.*, **22**, 1665–1668.
- Schulte-Pelkum, V., Monsalve, G., Sheehan, A., Pandey, M.R., Sapkota, S., Bilham, R. & Wu, F., 2005. Imaging the Indian subcontinent beneath the Himalaya, *Nature*, **435**, 1222–1225.
- Sipkin, S.A., 1982. Estimation of earthquake source parameters by the inversion of waveform data: synthetic waveforms, *Phys. Earth Planet. Inter.*, **30**, 242–259.
- Stich, D., Ammon, C.J. & Morales, J., 2003. Moment tensor solutions for small and moderate earthquakes in the Ibero-Maghreb region, *J. Geophys. Res.-Solid Earth*, **108**, ESE 7.
- Stich, D., Mancilla, F.D. & Morales, J., 2005. Crust-mantle coupling in the Gulf of Cadiz (SW-Iberia), *Geophys. Res. Lett.*, **32**, L13306.
- Velasco, A.A., et al., 2007. Using small, temporary seismic networks for investigating tectonic deformation: Brittle deformation and evidence for strike slip faulting in Bhutan, *Seismol. Res. Lett.*, **23**, 435–438.
- Wessel, P. & Smith, W.H.F., 1991. Free software helps map and display data, *Eos Trans. AGU*, **72**, 441.
- Yuan, X.H., Ni, J., Kind, R., Mechie, J. & Sandvol, E., 1997. Lithospheric and upper mantle structure of southern Tibet from a seismological passive source experiment, *J. Geophys. Res.-Solid Earth*, **102**, 27 491–27 500.
- Zhao, W.J. & Nelson, K.D., 1993. Deep seismic-reflection evidence for continental underthrusting beneath Southern Tibet, *Nature*, **366**, 557–559.
- Zhu, L.P. & Helmberger, D.V., 1996. Advancement in source estimation techniques using broadband regional seismograms, *Bull. Seismol. Soc. Am.*, **86**, 1634–1641.
- Zhu, L.P. & Helmberger, D.V., 1996. Intermediate depth earthquakes beneath the India-Tibet collision zone, *Geophys. Res. Lett.*, **23**, 435–438.

APPENDIX

Moment tensor inversion and first motion plot summaries for events not illustrated in main manuscript.

(a) Top left panel shows the misfit versus depth curves for models M1 and M2 and first motion polarity points plotted on the best



double-couple moment tensor solution. Numbers above each focal mechanism denote the non-double couple percentages for the solution at the associated depth. (b) Map shows the station locations used in the inversion relative to the epicentre. (c) Bottom panel shows the synthetic waveforms (dashed line) compared to the observed

waveforms at the global minimum misfit for the Radial (R), Transverse (T) and Vertical (V) components. On the first motion plots, black dots are compressional first arrivals, white circles are dilatational first arrivals, and '+' indicates emergent or undetermined first motion arrivals

